Nonlinear Kinetic Parameter Estimation for Batch Cooling Seeded Crystallization

Q. Hu, S. Rohani, D. X. Wang, and A. Jutan
Dept. of Chemical and Biochemical Engineering, University of Western Ontario, London, ON N6A 5B9, Canada

DOI 10.1002/aic.10163
Published online in Wiley InterScience (www.interscience.wiley.com).

Kinetic parameter estimation for most batch crystallization processes is necessary because nucleation and crystal growth kinetic parameters are often not available. The existing identification methods are generally based on simplified population balance models such as moment equations, which contain insufficient information on the crystal size distribution (CSD). To deal with these problems, a new optimization-based identification approach for general batch cooling seeded crystallization is proposed in this study. The final-time CSD is directly used for identification. A novel effective method for solving the population balance equation is developed and used to identify nucleation and growth kinetic parameters. Cooling crystallization of ammonium sulfate in water was experimentally investigated, where the concentration was measured by an on-line density meter and the final-time CSD was analyzed by a Malvern Mastersizer 2000. Kinetics for ammonium sulfate are determined based on cooling crystallization experiments. Applying these kinetics in simulation provides a good prediction of the product CSD. © 2004 American Institute of Chemical Engineers *AIChE J,* 50: 1786–1794, 2004
Keywords: model identification, batch crystallization, crystal size distribution, crystallization kinetics, ammonium sulfate

Introduction

Batch crystallization is widely used in the production of high value-added products, which are essentially characterized by the crystal size distribution (CSD). Usually, the final-time CSD of a batch crystallization determines product quality. In the case of batch cooling crystallization, the cooling rate affects the supersaturation profile and has strong influence on the CSD. Thus, optimization of temperature profiles is of great importance. A major obstacle for designing the optimal temperature profiles pertains to the accuracy of the mathematical models that highly depends on adequate representations of crystallization kinetics.

Garside et al. (1982) suggested a simple technique, known as initial derivatives, to deduce crystal growth kinetics from isothermal batch experiments performed in the integral model. This technique was extended to a batch cooling crystallizer (Tavare, 1985). Palwe et al. (1985) used three different methods, including polynomial fitting, initial derivatives, and optimization procedure, to determine the growth rate kinetics of ammonium nitrate. They noted that the least-squares error optimization procedure is potentially the most accurate and precise. Witkowski et al. (1990) implemented optimization-based estimation of crystallization kinetics by minimizing a weighted least-squares objective function, which represented the error between the estimated and experimental data. They used on-line concentration and transmittance data from a batch naphthalene–toluene system, in which the error weights are chosen arbitrarily. Qiu and Rasmuson (1991) used concentration and final-time CSD data to determine kinetic parameters for an aqueous succinic acid system. They simplified the population balance equation (PBE) to a first-order quasi-linear equation by assuming that the crystal growth rate can be expressed as a product of a function of supersaturation and a function of crystal size. Dash and Rohani (1993) estimated crystallization kinetics of potassium chloride. They included

Correspondence concerning this article should be addressed to S. Rohani at rohani@eng.uwo.ca.

crystal mass distribution from a sieve analysis in the objective function. Monnier et al. (1997) used calorimetry and image analysis to identify nucleation and growth kinetic parameters of adipic acid in water. Weighted least squares were also used by some other researchers to estimate kinetics in batch crystallization (David et al., 1991; Livk et al., 1995; Tadayyon et al., 2002). However, none of these researchers justified the selection of the weights. A maximum likelihood estimation (MLE) scheme was used by Miller (1993) to identify kinetic parameters from on-line concentration and transmittance measurements in a KNO_3–H_2O system. The similar strategy was used by Matthews and Rawlings (1998) for an organic photochemical–heptane system. Concentration and transmittance measurements were used for estimation. However, the concentration and transmittance measurements do not contain sufficient information to determine the CSD, and consequently the parameters determined by this method may not be satisfactory.

Most of the published methodologies used method of moments to reduce the population balance to a set of ordinary differential equations (ODEs) or changed the PBE to simple forms under some assumptions, so their applications are limited to cases such as size-independent growth rate and no fines dissolution. This article presents a new optimization-based methodology to identify kinetic parameters of batch crystallization using the final-time CSD analyzed by a Malvern Mastersizer 2000. A novel approach for solving the PBE is proposed and consequently size-dependent growth rates can be considered. To evaluate the effectiveness of this method, simulations and experimentations are performed. A good match between the predicted and actual CSD is obtained.

Model Formulation

A mathematical framework suited to modeling crystallization processes is the population balance, which describes the state of the CSD. If crystal agglomeration and breakage phenomena are neglected, the population balance for a batch cooling crystallizer is (Miller, 1993)

$$\frac{\partial f(L, t)}{\partial t} + \frac{\partial [G(L, t) f(L, t)]}{\partial L} = 0 \tag{1}$$

where f is the population density of crystals, G is the crystal growth rate, subject to the spatial boundary condition

$$f(0, t) = \frac{B^0}{G|_{L=0}} \tag{2}$$

where B^0 is the crystal nucleation rate at size zero.

The crystal growth rate is given by

$$G = k_g(T, L)(\Delta C)^{\alpha} \tag{3}$$

where $\Delta C = C - C_{sat}$. The crystal growth rate constant k_g is temperature dependent and it may also be dependent on the crystal size, which may be expressed by

$$k_g(T, L) = k_0 \exp(-E_g/RT)(1 + k_1 L)^{k_2} \tag{4}$$

The nucleation rate may be expressed as

$$B^0 = k_b(\Delta C)^{\beta} \tag{5}$$

Under the assumption that the slurry volume remains constant during the crystallization, the mass balance for the batch cooling crystallizer is

$$\frac{dC}{dt} = -\rho k_v \frac{d\mu_3}{dt} \tag{6}$$

where μ_3 is the 3rd moment of the CSD, defined as

$$\mu_3 = \int_0^{\infty} f L^3 dL \tag{7}$$

The energy balance is not required to simulate the crystallizer because the measurements of slurry temperature are assumed to be available. The necessary initial conditions for the population and mass balances, respectively, are

$$f(L, t) = f_0(L) \qquad t = 0 \tag{8}$$

$$C(t) = C_0 \qquad t = 0 \tag{9}$$

The model is identified by estimating the parameters in Eqs. 3 and 5 from experimental data. The parameters to be estimated include E_g, k_0, k_1, k_2, k_b, α, and β.

Model Solution

The PBE described in the previous section is a hyperbolic partial differential equation (PDE). Analytical solution of the PBE does not exist, and the numerical solution of the model is necessary to estimate the parameters.

The concept of population balance has been a major contribution to the subject of crystallizer analysis and design. A representation of population balance is shown in Figure 1, where population balance distributions at time $t = t_0$ and $t = t_0 + \Delta t$ are demonstrated. The crystals grow into the size range $L_2 + \Delta L_2$ from size range $L_1 + \Delta L_1$ over the time interval Δt. $f_0 = f(L_1, t_0)$ and $f_1 = f(L_2, t_0 + \Delta t)$ represent the population density at time t_0 and $t_0 + \Delta t$, respectively. Without crystal agglomeration and breakage phenomena, the population balance implies

$$f(L_1, t_0)\Delta L_1 = f(L_2, t_0 + \Delta t)\Delta L_2 \tag{10}$$

Based on the definition of growth rate,

$$L_2 \approx L_1 + G(L_1, t_0)\Delta t \tag{11}$$

$$L_2 + \Delta L_2 \approx L_1 + \Delta L_1 + G(L_1 + \Delta L_1, t_0)\Delta t \tag{12}$$

we have

$$\Delta L_2 \approx \Delta L_1 + [G(L_1 + \Delta L_1, t_0) - G(L_1, t_0)]\Delta T$$

$$\approx \left[1 + \frac{\partial G(L_1, t_0)}{\partial L}\Delta t\right]\Delta L_1 \tag{13}$$

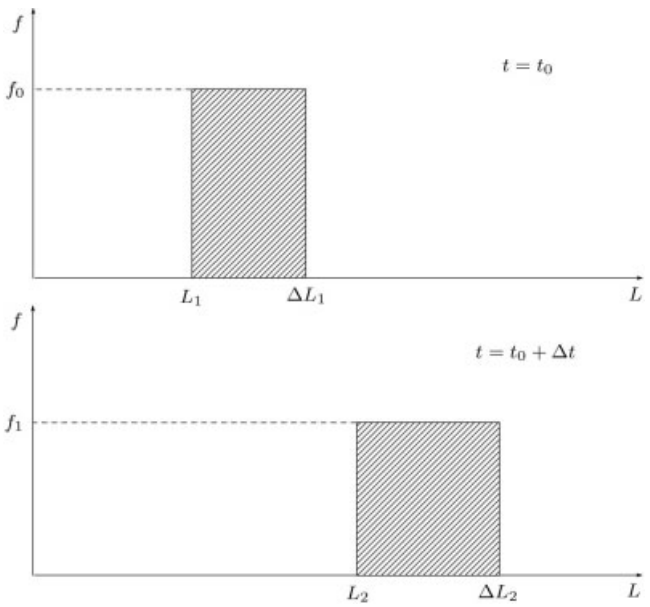

Figure 1. Representation of population balance.

$$f(L_2, t_0 + \Delta t) \approx f(L_1, t_0 + \Delta t) + \frac{\partial f(L_1, t_0 + \Delta t)}{\partial L} G(L_1, t_0)\Delta t \tag{14}$$

Substituting Eqs. 13 and 14 into Eq. 10 gives

$$f(L_1, t_0) \approx f(L_1, t_0 + \Delta t) + \frac{\partial f(L_1, t_0 + \Delta t)}{\partial L} G(L_1, t_0)\Delta t + f(L_1, t_0 + \Delta t) \frac{\partial G(L_1, t_0)}{\partial L} \Delta t + \frac{\partial f(L_1, t_0 + \Delta t)}{\partial L} \frac{\partial G(L_1, t_0)}{\partial L} G(L_1, t_0)(\Delta t)^2 \tag{15}$$

which can be written as

$$\frac{f(L_1, t_0 + \Delta t) - f(L_1, t_0)}{\Delta t} \approx -G(L_1, t_0) \frac{\partial f(L_1, t_0 + \Delta t)}{\partial L} - f(L_1, t_0 + \Delta t) \frac{\partial G(L_1, t_0)}{\partial L} + \frac{\partial f(L_1, t_0 + \Delta t)}{\partial L} \frac{\partial G(L_1, t_0)}{\partial L} G(L_1, t_0)\Delta t \tag{16}$$

If $\Delta t \rightarrow 0$, Eq. 16 becomes

$$\frac{\partial f(L, t)}{\partial t} = -G(L, t) \frac{\partial f(L, t)}{\partial L} - f(L, t) \frac{\partial G(L, t)}{\partial L} \tag{17}$$

which is equivalent to Eq. 1. Therefore, we can use the idea represented in Figure 1 to solve Eq. 1.

For description of the CSD in a batch crystallizer, we can apply the conservation law of numbers of crystals and the concept of population balance as well. In this method, the batch time period is divided into n time steps, each with length Δt. The density function f is a representation of the number of crystals in a given size range and a given volume. As shown in Figure 2, at the time $t = j\Delta t$, we arbitrarily choose $m + 1$ points where we may want to calculate the population density for the time $t = (j + 1)\Delta t$, with the size $L_{j,0}, L_{j,1}, \ldots, L_{j,m}$ and population densities $f_{j,0}, f_{j,1}, \ldots, f_{j,m}$. The first index ($j = 0, 1, \ldots, n$) denotes the time interval number and the second index indicates the series number of points of the CSD. Let us consider the point $(L_{j,i}, f_{j,i})$. When breakage and agglomeration are neglected, the number of crystals in the size range $L_{j,i}$ to $L_{j,i} + \Delta L_{j,i}$ remains constant, that is

$$\int_{L_{j,i}}^{L_{j,i}+\Delta L_{j,i}} f(L, t)dL = \int_{L_{j+1,i}}^{L_{j+1,i}+\Delta L_{j+1,i}} f(L, t)dL \tag{18}$$

Using a simple first-order approximation provides

$$\int_{L_{j,i}}^{L_{j,i}+\Delta L_{j,i}} f(L, t)dL = \Delta L_{j,i} f_{j,i} + \bigcirc(\Delta L_{j,i}) \tag{19}$$

The quantity $\bigcirc(\Delta L_{j,i})$ represents the asymptotic notation for the truncation error of this approximation. Using the definition of growth rate gives

$$G(L_{j,i}, j)\Delta t = L_{j+1,i} - L_{j,i} + \bigcirc(\Delta t) \tag{20}$$

$$G(L_{j,i} + \Delta L_{j,i}, j)\Delta t = L_{j+1,i} - L_{j,i} + \Delta L_{j+1,i} - \Delta L_{j,i} + \bigcirc(\Delta t) \tag{21}$$

By use of Eqs. 20 and 21, we obtain

$$\Delta L_{j+1,i} = \Delta_{j,i} + [G(L_{j,i} + \Delta L_{j,i}, j) - G(L_{j,i}, j)]\Delta t + \bigcirc(\Delta t) \tag{22}$$

Substituting Eq. 22 into Eqs. 18 and 19 yields

$$f_{j+1,i} = \frac{\Delta L_{j,i} f_{j,i}}{\Delta L_{j,i} + [G(L_{j,i} + \Delta L_{j,i}, j) - G(L_{j,i}, j)]\Delta t} + \bigcirc(\Delta t + \Delta L_{j,i}) \tag{23}$$

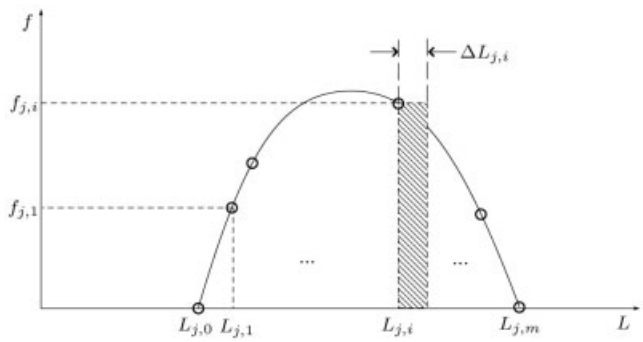

Figure 2. Population density discretization.

which emphasizes the local truncation error. If $\Delta L_{j,i}$ goes to zero, Eq. 23 becomes

$$f_{j+1,i} = \frac{f_{j,i}}{1 + \left.\frac{\partial G(L, t)}{\partial L}\right|_{L=L_{j,i},t=j\Delta t} \Delta t} + \bigcirc(\Delta t) \tag{24}$$

If Δt is sufficiently small, an approximation can be obtained

$$\tilde{f}_{j+1,i} = \frac{\tilde{f}_{j,i}}{1 + \left.\frac{\partial G(L, t)}{\partial L}\right|_{L=L_{j,i},t=j\Delta t} \Delta t} \tag{25}$$

The difference equation for

$$z_{i,j} = f_{i,j} - \tilde{f}_{i,j} \tag{26}$$

is obtained by subtracting Eq. 25 from Eq. 24; thus

$$z_{j+1,i} = \frac{z_{j,i}}{1 + \left.\frac{\partial G(L, t)}{\partial L}\right|_{L=L_{j,i},t=j\Delta t} \Delta t} + \bigcirc(\Delta t) \tag{27}$$

Given that f agrees with $\tilde{f}$ initially and on the boundary

$$z_{0,i} = 0 \qquad i = 0, 1, \ldots, m \tag{28}$$

$$z_{j,0} = z_{j,m} = 0 \qquad j = 0, 1, \ldots, n \tag{29}$$

The definition of growth rate implies

$$\left.\frac{\partial G(L, t)}{\partial L}\right|_{L=L_{j,i},t=j\Delta t} \geq 0 \tag{30}$$

and therefore

$$\left| \frac{1}{1 + \left.\frac{\partial G(L, t)}{\partial L}\right|_{L=L_{j,i},t=j\Delta t} \Delta t} \right| \leq 1 \tag{31}$$

Then from Eq. 27 we obtain

$$|z_{j+1,i}| \leq |z_{j,i}| + A[\Delta t] \tag{32}$$

and because $z_{0,i} = 0$ we easily calculate that

$$\begin{aligned} |z_{j+1,i}| &\geq A(j + 1)[\Delta t] \\ &\leq AT[\Delta t] \end{aligned} \tag{33}$$

given that $(j + 1)\Delta t \leq T$.

Equation 33 means that the error $z_{i,j}$ approaches zero as Δt approaches zero. Thus the solution of the finite-difference analog converges to the solution of the PBE as Δt approaches zero. The boundedness condition implies stability (Ames, 1969). It should be noted that Eqs. 24–33 are independent of $\Delta L_{i,j}$.

Table 1. Kinetic Parameters for Model Simulations

Parameter	Value	Units
E_g	6.19×10^4	J mol^{-1}
k_0	4.31×10^7	m min^{-1}
k_1	1.0×10^3	m^{-1}
k_2	0.80	Dimensionless
k_b	7.78×10^5	Crystal number kg^{-1} min^{-1}
α	0.91	Dimensionless
β	0.90	Dimensionless

Because the seed size distribution is assumed to be known, $f_{0,i}$ and $L_{0,i}$ are available. Therefore, $f_{j+1,i}$, for $j = 0, 1, \ldots, n - 1$ and $i = 0, 1, \ldots, m - 1$, can be solved iteratively by Eq. 25. Based on Eq. 20

$$L_{j+1,i} \approx G(L_{j,i}, j)\Delta t + L_{j,i} \tag{34}$$

and $L_{j+1,i}$ can be solved iteratively using Eq. 34 as well.

If the growth rate is size-independent (that is, $\partial G/\partial L = 0$), then $f_{j+1,i} = f_{j,i}$, for $i = 0, 1 \ldots, m - 1, j = 0, 1, \ldots, n - 1$. In this case, the seed distribution does not change shape, and it simply moves out along the L axis at a rate equal to $G(L_{j,0}, j)$. In the case of size-dependent growth rate, the integral of seed distribution over L is constant in the absence of agglomeration and breakage.

This method provides a means to reduce the PBE to a set of algebraic equations. These equations can be easily solved along with the mass balance equation. By assuming that the secondary nuclei have the same growth behavior as that of the seed crystals, and using the same method, we can obtain

$$f^N_{j+1,i} \approx \frac{f^N_{j,i-1}}{1 + \left.\frac{\partial G(L, t)}{\partial L}\right|_{L=L^N_{j,i-1},t=j\Delta t} \Delta t} \tag{35}$$

for $j = 0, 1, \ldots, n - 1$ and $i = 1, 2, \ldots, j + 1$, with the boundary conditions of Eq. 2 and $L_{j,0} = 0$.

To illustrate this solution technique, simulations were performed for a hypothetical chemical system, where the kinetic parameters are given in Table 1, and the solubility of the solute in the solvent is given by

$$C_{\text{sat}} = 0.0016T^2 + 0.1871T + 70.9943 \quad \text{(g solute/100 g solvent)} \tag{36}$$

where T is in °C. The density of the crystals is $\rho = 1.77$ g/cm^3, and the shape factor was taken to be $k_v = 1$. The solvent and the seed loads were taken to be 1500 and 2.5 g, respectively. A temperature profile of constant cooling rate from 30 to 10°C in 1 h was imposed. The initial solute concentration was taken to be 0.8 g solute/g solvent.

One of the simulation results shown in Figure 3 is the time evolution of the CSD. The resulting concentration is shown in Figure 4. The seed and newly formed crystal size distribution is given in Figure 5.

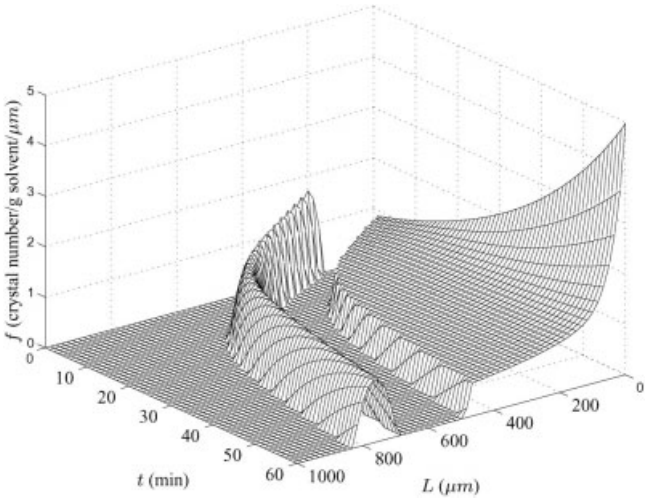

Figure 3. Evolution of CSD for the simulation model.

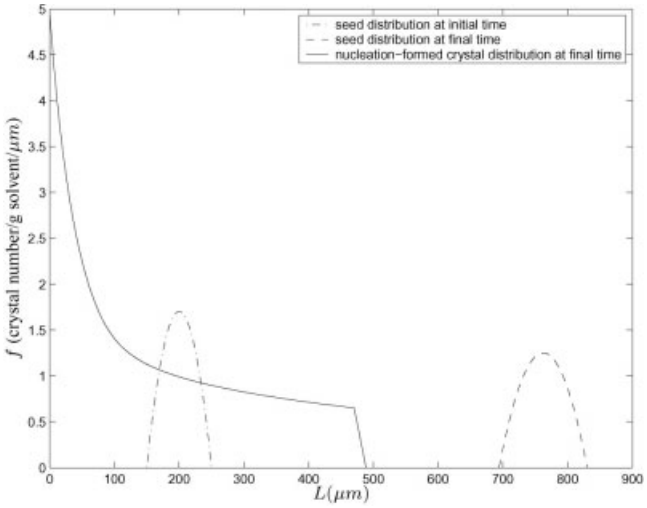

Figure 5. Seed and newly formed crystal size distribution.

The orthogonal collocation method is very efficient for solving differential equations (Villadsen and Michelsen, 1978). Miller (1993) discussed the use of orthogonal collocation to solve the PBE. The method approximates the solution as a linear combination of basis functions and requires that the approximation satisfies the differential equation at the collocation points. The function $f(L, t)$ can be approximated by a linear combination of Lagrange interpolation polynomials, that is

$$f(L, t) \approx \sum_{j=1}^{l} f(L_j, t)\ell_j(L) \tag{37}$$

where ℓ_j is the Lagrange interpolation polynomial of degree j, and $f(L_j, t)$ is the function evaluated at the point L_j. The approximation of the derivative with respect to L can be written as

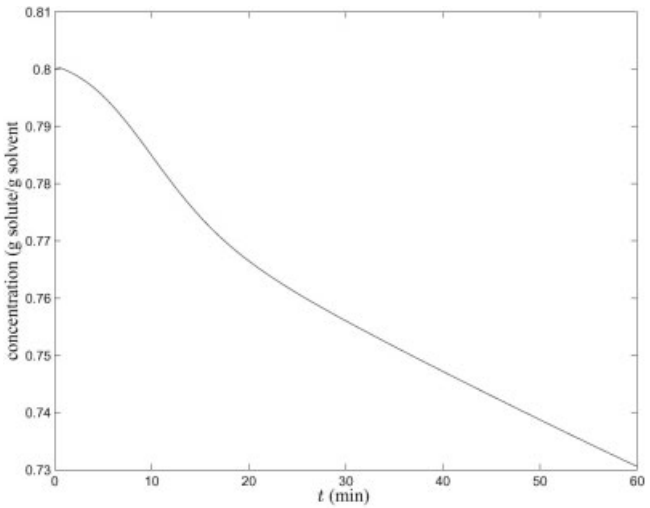

Figure 4. Concentration for the simulation model.

$$\frac{\partial f}{\partial L} \approx \sum_{j=1}^{l} f(L_j, t)\,\frac{d\ell_j(L)}{dL} \tag{38}$$

Thus

$$\left.\frac{\partial f}{\partial L}\right|_{L=L_i} \approx \sum_{j=1}^{l} A_{ij} f(L_j, t) \tag{39}$$

where

$$A_{ij} = \left.\frac{d\ell_j}{dL}\right|_{L_i} \tag{40}$$

Orthogonal collocation with Lagrange polynomials is based on Eqs. 38–40. Identical results, as shown in Figures 3–5, were obtained by using this orthogonal collocation solution technique for the simulation example.

Parameter Estimation

If we define the error e_{ij} as the difference between the measured and predicted values of a variable

$$e_{ij}(\boldsymbol{\theta}) = y_{ij}(\boldsymbol{\theta}) - \tilde{y}_{ij}(\boldsymbol{\theta}) \tag{41}$$

where $\tilde{y}$ denotes the predicted value, and a variable subscripted by ij denotes the jth value of the ith variable. The least-squares procedure consists of finding the values of $\boldsymbol{\theta}$ that minimize the function

$$\Phi(\boldsymbol{\theta}) = \sum_{i=1}^{N_m} \sum_{j=1}^{N_i} e_{ij}^2(\boldsymbol{\theta}) \tag{42}$$

That is, we minimize the sum of squares of the residuals. N_m is the number of variables and N_i is the number of measurements

of each variable. This method is a widely used estimation procedure. The objective function (Eq. 42), consisting of a simple sum of squares, is often unsatisfactory because of several reasons, such as different scales of measurement or various physical dimensions. Also, some observations may be known to be less reliable than others, and parameter estimates should be less influenced by those than by more accurate ones. The solution to these problems is the method of weighted least squares. Assign a nonnegative weight factor ω_{ij} to each $e_{ij}(\theta)$, and minimize

$$\Phi(\boldsymbol{\theta}) = \sum_{i=1}^{N_m} \sum_{j=1}^{N_i} \omega_{ij} e_{ij}^2(\boldsymbol{\theta}) \tag{43}$$

A small ω_{ij} is chosen for y_{ij}, which is measured on a large scale, or which are highly unreliable, and conversely for large ω_{ij}. Statistical information may be required such that the weights can be chosen to incorporate data error structure. However, the weights are usually set somewhat arbitrarily because statistical information is often not available (Miller, 1993).

The maximum likelihood method provides a means to estimate the weights. If the model equations are linear in the parameters, or if the number of observations is large and the errors are normally distributed, then the choice of weights leading to least-variance estimates is given by the elements of the inverse of the covariance matrix of the errors (Bard, 1974). When the covariance matrix is not known, the maximum likelihood method can be chosen to estimate the weights along with the other parameters. We consider the case of a normal distribution with the typical assumptions: (1) All errors are independent. (2) Errors of each measurement are normally distributed with zero mean. In this case, the maximum likelihood method is equivalent to minimizing

$$\Phi(\boldsymbol{\theta}) = \sum_{i=1}^{N_m} \frac{N_i}{2} \ln\left(\sum_{j=1}^{N_i} e_{ij}^2(\boldsymbol{\theta}) \right) \tag{44}$$

and the estimates of the elements of the covariance matrix are

$$\hat{\mathbf{V}}_{ii} = \frac{1}{N_i} \sum_{j=1}^{N_i} e_{ij}^2(\boldsymbol{\theta}) \tag{45}$$

where $\mathbf{V}$ is an $N_m \times N_m$ matrix. Thus, the two steps for the maximum likelihood method are as follows:

(1) Find $\boldsymbol{\theta}^*$ to minimize $\Phi(\boldsymbol{\theta})$.

(2) Estimate $\mathbf{V}^* = \hat{\mathbf{V}}(\boldsymbol{\theta}^*)$ from Eq. 45.

The case considered here may be regarded as solving the weighted least-squares problems with unknown weights.

Therefore, the optimal parameter values are found by solving the nonlinear optimization problem

$$\min_{\theta} \Phi(\boldsymbol{\theta})$$

subject to: Conditions 1–9.

It is not enough to compute a vector $\boldsymbol{\theta}^*$ and to state this is the estimated value of the unknown parameter $\boldsymbol{\theta}$. The reliability and precision of the estimates must be investigated. If the model equations can be approximated by linear ones in the vicinity of the estimate $\boldsymbol{\theta}^*$, the model may be approximated by

$$\tilde{y}_{ij}(\boldsymbol{\theta}) \approx \tilde{y}_{ij}(\boldsymbol{\theta}^*) + \Gamma_{ij}(\boldsymbol{\theta} - \boldsymbol{\theta}^*) \tag{46}$$

where

$$\Gamma_{ij} = \left. \frac{\partial y_{ij}}{\partial \boldsymbol{\theta}} \right|_{\boldsymbol{\theta}=\boldsymbol{\theta}^*} \tag{47}$$

is a $1 \times p$ vector. It can be proved that the vector $\boldsymbol{\theta} - \boldsymbol{\theta}^*$ has covariance

$$\mathbf{V}_{\boldsymbol{\theta}} = \left(\sum_{i=1}^{N_m} \sum_{j=1}^{N_i} \Gamma_{ij}^T \mathbf{V}^{-1} \Gamma_{ij} \right)^{-1} \tag{48}$$

If the errors in the observations are normally distributed, so are the estimates $\boldsymbol{\theta}^*$; and therefore, the quantity

$$\varkappa \equiv (\boldsymbol{\theta} - \boldsymbol{\theta}^*)^T \mathbf{V}_{\boldsymbol{\theta}}^{-1} (\boldsymbol{\theta} - \boldsymbol{\theta}^*) \tag{49}$$

is distributed as χ^2 with p degrees of freedom; that is

$$P\{\varkappa \leq \chi_p^2(a)\} = 1 - a \tag{50}$$

where P denotes the probability. Hence, we can determine confidence regions for $\boldsymbol{\theta}^*$ with the measurement error covariance matrix $\mathbf{V}$. The approximate $100(1 - a)\%$ confidence region is defined by

$$(\boldsymbol{\theta} - \boldsymbol{\theta}^*)^T \mathbf{V}_{\boldsymbol{\theta}}^{-1} (\boldsymbol{\theta} - \boldsymbol{\theta}^*) = \chi_p^2(a) \tag{51}$$

The above discussion was based on the assumption that the model equations were nearly linear in the parameters around the estimate $\boldsymbol{\theta}^*$, and consequently the linearity assumption should be tested.

Experimental Work

The experiments with ammonium sulfate were performed in a stirred double-jacketed crystallizer with a volume of about 1.5 L; a density meter for on-line concentration measurement; a chiller (HX-150, Thermo Neslab Instruments), which can manipulate the jacket water temperature according to the set point value; a stirrer driven by a motor; and a thermocouple to measure the temperatures of crystallizer and jacket. Additional elements of the system include data acquisition and control hardware and a computer that performs on-line control calculations and stores the collected data. A schematic of the experimental apparatus is shown in Figure 6, where T is in °C. The density of $(NH_4)_2SO_4$ is $\rho = 1.77$ g/cm^3. The shape factor was taken to be $k_v = 1$.

The temperature-control system uses a chiller to allow fast changes in jacket water temperature. The objective of the control system is to control the temperature of the contents of the crystallizer. The control is accomplished through a cascade

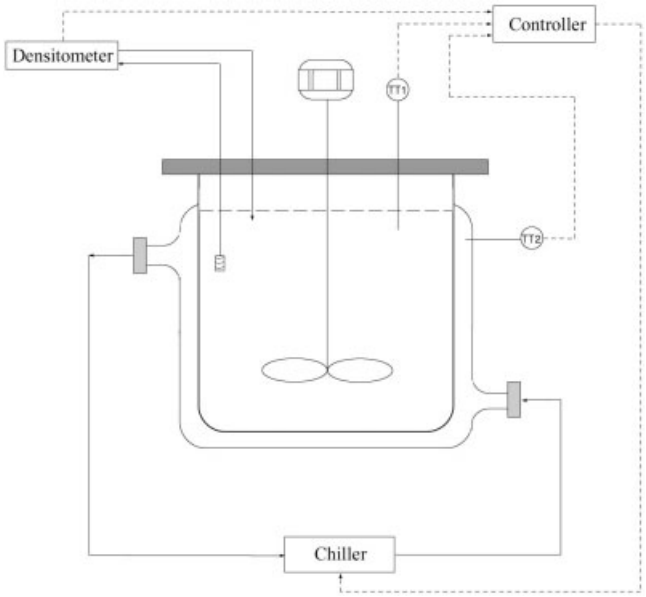

Figure 6. Experimental apparatus.

design. A PI controller compares an on-line measurement of the crystallizer temperature to a preprogrammed set point temperature and then calculates an appropriate corrective value for the temperature of the incoming jacket water. This value is passed, as a new set point, to a PI slave controller that adjusts the set point to the chiller to meet the new goal. Parameters of the PI controllers were carefully selected. The temperature-control system had the capacity to follow accurately and precisely a given temperature profile.

Three temperature profiles used in the cooling crystallization experiments are shown in Figure 7, where the temperature range was selected to be 30–10°C over a 1.5-h batch time. Each of these profiles was replicated at least twice. The only differences among the replicates were the random noise in the temperature profiles. The temperature of the crystallizer was measured at 10-s intervals throughout a crystallization run. The time delay for the temperature measurement was negligible.

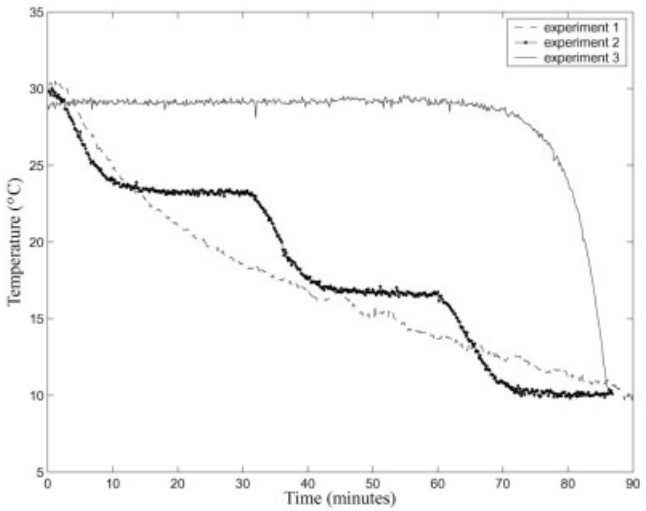

Figure 7. Temperature profiles for batch crystallization.

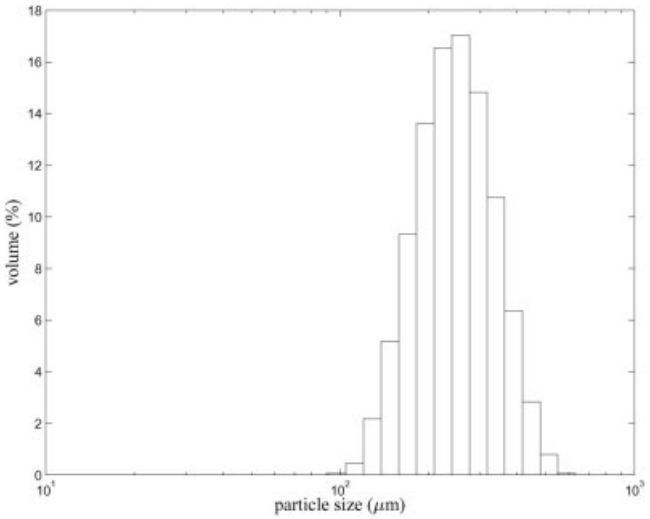

Figure 8. CSD of seed.

The solubility curve for ammonium sulfate within this temperature range is (Mullin and Nyvlt, 1971)

$$C_{sat} = 0.00225T + 0.704 \tag{52}$$

The crystallizer was charged with initial loads of solvent and solute constituting the desired solute concentration. Typical charges were 624 g of ammonium sulfate and 800 g of water. These were measured on a high-capacity electronic balance. The initial concentration was 0.78 g of ammonium sulfate per gram of water, providing a 1°C cushion between the highest operating temperatures and saturation temperature of the initial solution. The initial supersaturation is 0.0022, which is within the metastable zone of ammonium sulfate and consequently primary nucleation is not expected (Mullin and Nyvlt, 1971). The solution was maintained initially at about 36°C, which is approximately 5°C above the saturation temperature of the solution. The crystallizer was maintained at this temperature for about 15 min after dissolution appears to be complete. The crystallizer was cooled to 30°C by adjusting the set point of the cascade PID controller. This temperature was maintained for about 15 min. The mass of the seed load was measured on an electronic balance with a 0.0001-g precision. Seed crystals of mean size 255.5 μm were prepared from the commercial product by recrystallization and careful sieving. The seed distribution is shown in Figure 8. Seed loads in this study were 10 g ($\sim$5.7346 $\times$ 10^5 crystals). The stirrer speed was 7 rps.

The final-time product was immediately filtered using a 5-micron filter paper. To avoid agglomeration upon drying, the crystals were then washed with isopropanol saturated with ammonium sulfate. The wet crystals on the filter paper were collected and immediately used for size analysis. Isopropanol solution saturated with ammonium sulfate was used as the suspension liquid for the CSD measurement with a Malvern Mastersizer. Before each measurement, the 500-mL suspension chamber of the Mastersizer sensing zone and the connecting tubes were rinsed and then filled with the suspension liquid. Suitable amounts of the product ($\sim$5 g) were added to the chamber, vibrated for 20 s with ultrasound before size distribution measurement.

Table 2. Parameter Estimates and 95% Confidence Intervals

Parameter	Estimate	Confidence Interval
$\ln(E_g)$	11.18	± 0.22
$\ln(k_0)$	13.99	± 0.24
$\ln(k_1)$	14.60	± 0.27
k_2	0.87	± 0.04
$\ln(k_b)$	13.45	± 0.23
α	0.82	± 0.03
β	0.91	± 0.04

As mentioned earlier, for a cooling crystallization process the states of interest are the CSD, the concentration of the crystallizing solute in the liquid phase, and the system temperature. The CSD describes the state of the solid phase and the product quality. Temperature profile and initial concentration specify the driving force in the system. Although it is not possible to measure the CSD explicitly on-line, we can obtain the final-time CSD using a Malvern Mastersizer. It was found that density is not a sufficiently sensitive property for determination of the concentration of ammonium sulfate solutions, and the on-line concentration measurement of the experiments is not reliable; thus, we use only the final-time CSD, temperature profile, and the initial concentration to estimate the kinetics of ammonium sulfate.

The batch time period was dividend into n time steps, and the CSD of the seed was divided into m groups, with the size intervals $\Delta L_{0,0}$, $\Delta L_{0,1}$, . . . , $\Delta L_{0,m-1}$ and population densities $f_{0,0}, f_{0,1}, \ldots, f_{0,m}$, respectively. Because the final-time CSD of the product is available, we can also divide the final-time seed distribution into m groups, such that $\Delta L_{0,0} f_{0,0} = \Delta L_{n,0} f_{n,0}$, $\Delta L_{0,1} f_{0,1} = \Delta L_{n,1} f_{n,1}, \ldots, \Delta L_{0,m-1} f_{0,m-1} = \Delta L_{n,m-1} f_{n,m-1}$. The final-time CSD for nucleated crystals was also divided into n equivalent groups. The objective of the optimization problem is

$$\Phi(\theta) = \frac{m}{2} \ln\left[\sum_{i=0}^{m-1} (f_{n,i} - \hat{f}_{n,i})^2\right] + \frac{n}{2} \ln\left[\sum_{j=0}^{n-1} (f^N_{n,j} - \hat{f}^N_{n,j})^2\right] \quad (53)$$

and the conditions

$$|L_{n,0} - \hat{L}_{n,0}| \leq \varepsilon_1 \quad (54)$$

$$|L_{n,m-1} - \hat{L}_{n,m-1}| \leq \varepsilon_2 \quad (55)$$

and

$$|L^N_{n,n} - \hat{L}^N_{n,n}| \leq \varepsilon_3 \quad (56)$$

where ε_1, ε_2, and ε_3, which are small positive slack constants chosen arbitrarily, become the constraints of the optimization problem. Ideally, ε_1, ε_2, and ε_3 should be zero. It should be noted that only the final-time population densities are included in the objective function because the product CSD can be totally determined by the population densities and the conditions in Eqs. 54–56. The estimates are presented in Table 2. The confidence intervals indicate that the parameters are well determined. The least-certain parameters are k_2 and k_n with intervals representing 4.94 and 3.66% of the parameter magnitudes, respectively. The other parameters are even more accurate with relative confidence intervals of less than 2%. It is found that the linearity assumption is valid in this problem, given that the actual values of the objective function at selected points on the boundary of the region differ only slightly from the approximation. A comparison of the simulated and experimental results for temperature profile 2 is shown in Figure 9. The CSD of the product clearly indicates the product composed of seeded crystals and newly formed crystals. The predicted and experimental CSD match very well, and only small discrepancies are observed. The small confidence region and high similarity between the predicted and experimental CSD were indications that the model was well identified over the desired operating region. A good match between simulated and actual CSD for temperature profiles 1 and 3 was obtained but is not shown here because of limited space.

The order of the growth rate with respect to supersaturation, as presented in Table 2, is 0.82. Comparable growth kinetic results (~0.8–1.1) were reported by Mullin et al. (1970) and Tavare (1985). The activation energy is about 72 kJ/mol, which is slightly higher than that obtained by Tavare (1985) (62 kJ/mol). Although the stirrer speed is fixed in our experiments, the overall growth rates estimated by this method (~0.005–0.18 μm/s) over the range of variables are comparable to those (~0.005–0.25 μm/s) derived from batch experiments or con-

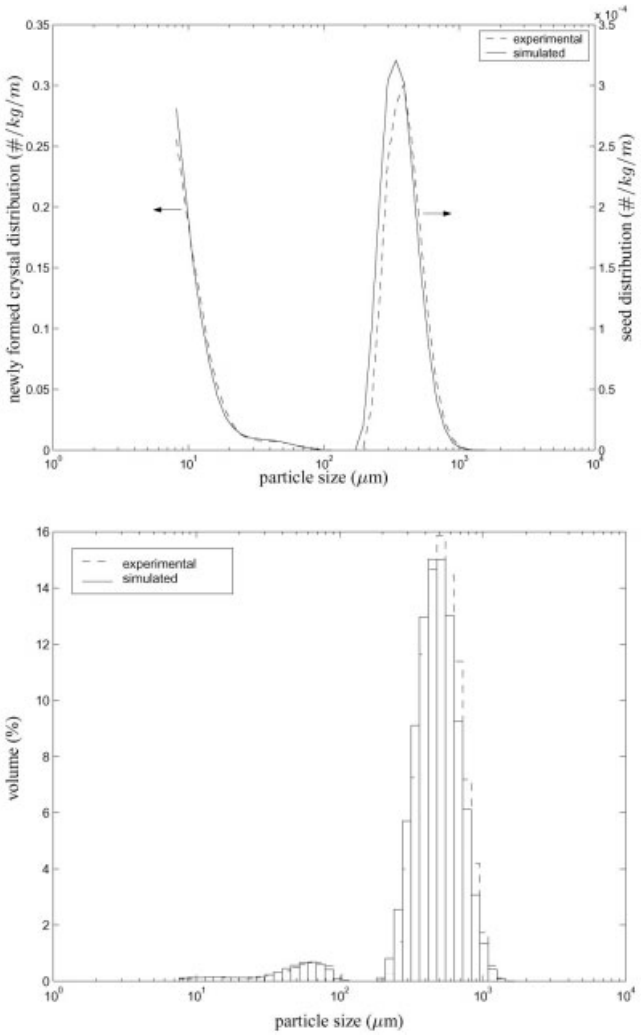

Figure 9. Experimental vs. simulated CSDs.

tinuous MSMPR crystallizer experiments by Larson and Mullin (1973) and Tavare (1985).

Conclusions

An approach to estimate the kinetic parameters of crystal nucleation and growth from batch cooling experiments is presented. The kinetic parameters were estimated using the final-time product CSD, the initial concentration and the experimental temperature profile collected on-line in the batch crystallization process. The parameter estimates were analyzed with respect to different experimental data. The reliability and precision of our estimates were investigated by giving the 95% confidence interval. In comparison to other techniques reviewed herein, the proposed method is significantly more efficient. Further, the kinetics are related directly to the CSD of the final-time product, instead of relying on insufficient and uncertain information of the crystals such as transmittance data. In comparison to batch techniques based on on-line concentration measurement, the present method has the advantage of being less sensitive to the accuracy and noises of the measurement. Using the method proposed, the growth rates for ammonium sulfate are determined and experimentally evaluated. Kinetic parameters reported herein are in good agreement with results previously published by other researchers.

Notation

B^0 = nucleation rate, number per kg solvent s^{-1}
C = concentration, kg solute per kg solvent
C_{sat} = saturation concentration, kg solute per kg solvent
ΔC = supersaturation, kg solute per kg solvent
E_g = activation energy for growth process, J mol^{-1}
f = crystal number density, number per kg of solvent m^{-1}
G = crystal growth rate, m/s
k_0, k_1, k_2 = constants in Eq. 4
k_b = nucleation constant
k_g = growth rate constant, m s^{-1}
k_v = volume shape factor
L = crystal size, m
p = number of parameters
R = gas constant, J mol^{-1} K^{-1}

Greek letters

α = growth order
β = nucleation order
μ_3 = 3rd moment of the CSD
ρ = density, g cm^{-3}
$\boldsymbol{\theta}$ = vector of model parameter

Subscripts

k_0, k_1, k_2 = initial
i, j = summation subscripts
m = group number of CSD
n = time steps of batch time
sat = saturated

Superscript

N = nucleated

Literature Cited

Ames, W. F., *Nonlinear Methods for Partial Differential Equations*, Thomas Nelson and Sons, Walton-on-Thames, UK (1969).

Bard, Y., *Nonlinear Parameter Estimation*, Academic Press, New York (1974).

Dash, S. R., and S. Rohani, "Iterative Parameter Estimation for Extraction of Crystallization Kinetics of Potassium Chloride from Batch Experiments," *Can. J. Chem. Eng.*, **71**, 539 (1993).

David, R., J. Villermaux, P. Marchal, and J. P. Klein, "Crystallization and Precipitation Engineering—4. Kinetic Model of Adipic Acid Crystallization," *Chem. Eng. Sci.*, **46,** 1129 (1991).

Garside, J., L. Gibilaro, and N. Tavare, "Evaluation of Crystal Growth Kinetics from Desupersaturation Curve Using Initial Time Derivatives," *Chem. Eng. Sci.*, **37**, 1625 (1982).

Larson, M. A., and J. W. Mullin, "Crystallization Kinetics of Ammonium Sulphate," *J. Crystal Growth*, **20**, 183 (1973).

Livk, I., M. Gregorka, and C. Pohar, "Identification of Batch Crystallization Processes (Estimate of Kinetic Parameters of Sodium-Perborate Precipitation," *Comput. Chem. Eng.*, **19,** S241 (1995).

Matthews, H. B., and J. B. Rawlings, "Batch Crystallization of a Photochemical: Modeling, Control, and Filtration," *AIChE J.*, **44**, 1119 (1998).

Miller, S. M., "Modelling and Quality Control Strategies for Batch Cooling Crystallizers," PhD Thesis, University of Texas at Austin (1993).

Monnier, O., G. Fevotte, C. Hoff, and J. Klein, "Model Identification of Batch Cooling Crystallization through Calorimetry and Image Analysis," *Chem. Eng. Sci.*, **52**, 1125 (1997).

Mullin, J. W., M. Chakraborty, and K. Mehta, "Nucleation and Growth of Ammonium Sulphate Crystals from Aqueous Solution," *J. Appl. Chem.*, **20**, 367 (1970).

Mullin, J. W., and J. Nyvlt, "Programmed Cooling of Batch Crystallizers," *Chem. Eng. Sci.*, **26**, 369 (1971).

Palwe, B. G., M. R. Chivate, and N. S. Tavare, "Growth Kinetics of Ammonium Nitrate Crystals in a Draft Tube Baffled Agitated Batch Crystallizer," *Ind. Eng. Chem. Process Des. Dev.*, **24**, 914 (1985).

Qiu, Y., and A. C. Rasmuson, "Nucleation and Growth of Succinic Acid in a Batch Cooling Crystallizer," *AIChE J.*, **37**, 1293 (1991).

Tadayyon, A., S. Rohani, and M. Bennett, "Estimation of Nucleation and Growth Kinetics of Ammonium Sulfate from Transients of a Cooling Batch Crystallizer," *Ind. Eng. Chem. Res.*, **41**, 6181 (2002).

Tavare, N. S., "Growth Kinetics of Ammonium Sulfate in a Batch Cooling Crystallizer Using Initial Derivatives," *AIChE J.*, **31**, 1733 (1985).

Villadsen, J., and M. L. Michelsen, *Solution of Differential Equation Models by Polynomial Approximation*, Prentice-Hall, Englewood Cliffs, NJ (1978).

Witkowski, W. R., S. M. Miller, and J. B. Rawlings, "Light Scattering Measurements to Estimate Kinetic Parameters of Crystallization," *Crystallization as a Separations Process*, S. Myerson and K. Toyokura, eds., American Chemical Society, Washington, DC, pp. 102–114 (1990).

Manuscript received Jul. 28, 2003, and revision received Nov. 20, 2003.